Available online at www.sciencedirect.com
SCIENCE DIRECT
Journal of the European Ceramic Society 26 (2006) 1107–1119
www.elsevier.com/locate/jeurceramsoc

Mullite formation from the pyrolysis of aluminium-loaded polymethylsiloxanes: The influence of aluminium powder characteristics

Juliana Anggono [1], Brian Derby *

University of Manchester, School of Materials, Grosvenor Street, Manchester M1 7HS, UK

Received 17 October 2004; received in revised form 7 January 2005; accepted 10 January 2005
Available online 3 March 2005

Abstract

Polymethylsiloxane (PMS) filled with a range of aluminium powders of different size and morphology have been used to produce precursor mixtures to form mullite bodies. The size and shape of the Al powder is shown to have a strong influence on the temperature and mechanism of mullite formation, on the final microstructure and phase composition of the product. The reaction proceeds by decomposition of the PMS producing amorphous SiO_2. Al oxidation occurs both by reaction with the atmosphere and by reduction of the amorphous SiO_2 to produce α-Al_2O_3. Crystallisation of cristobalite was also observed prior to mullitisation. It is these components of the microstructure that react to produce mullite. The onset of mullite formation occurs at different temperatures, depending on the initial Al powder size and morphology. Large, flake morphology Al powders produced the greatest quantity of mullite and showed the lowest temperatures for mullite formation. XRD analysis identified 3:2 mullite in samples using large Al particles after heating to 1400 °C and at 1700 °C in samples using small Al powders.

Keywords: Mullite; Pyrolysis; Microstructure-prefiring; Microstructure-final

1. Introduction

Traditionally, mullite is produced by solid-state reaction between Al_2O_3 and SiO_2. However, this is limited by the low diffusion coefficients of the reacting species and the problems of achieving desired stoichiometry. Sol–gel routes can also be used to synthesise mullite but this leads to considerable shrinkage. This two-step process of synthesis followed by ceramic fabrication increases complexity and cost. For many non-oxide ceramics, pyrolysis of suitable polymers has been developed for the synthesis of ceramic materials. This method has many similarities with the sol–gel technique in that a complex, cross-linked macromolecular network is thermally transformed into a ceramic phase. In common with the sol–gel process, this requires the loss of substantial organic and other low molecular mass by-products, and leads to a considerable volume shrinkage.

Active-filler controlled pyrolysis (AFCOP) was first developed by Greil and co-workers.[1–4] In this process, a polymer that decomposes to a ceramic material is partially filled with active powder particles. These filler particles react with the decomposition products of the polymer or a reactive gas atmosphere, the volume expansion resulting from this reaction counters the shrinkage that occurs during sintering and allows the fabrication of bulk, near-net shape components.[4] This process can be used as a possible route to produce mullite by selecting a pre-ceramic polymer that decomposes to SiO_2 and using Al as the active filler.

The formation of mullite with low sintering shrinkage due to the positive specific-volume changes upon the oxidation of the polymer/filler components has been reported by

* Corresponding author. Tel.: +44 161 306 3569; fax: +44 161 306 3586.
E-mail address: brian.derby@manchester.ac.uk (B. Derby).
[1] Present address: Petra Christian University, Mechanical Engineering Department, Surabaya 60236, Indonesia.

0955-2219/$ – see front matter © 2005 Elsevier Ltd. All rights reserved.
doi:10.1016/j.jeurceramsoc.2005.01.052

Suttor et al.[5] Polymethylsiloxane (PMS), filled with Al powder (6.8 μm particle size) as the active-filler, was used as starting materials and mullite formation was reported at 1700 °C.[5] The same route was used by Michalet et al.[6] using polydimethylsiloxane (PDMS) filled with smaller sized Al particles (median size of 0.8 μm) and mullite was identified at temperatures as low as 1250 °C. Michalet et al. presented a detailed study of the evolution of phases during the pyrolysis of PDMS/Al and PDMS/Al_2O_3 mixtures. In summary, they proposed that the reaction proceeds by a complex series of reactions. In the presence of Al_2O_3, the PDMS undergoes thermal decomposition to amorphous SiO_2, this reacts with the Al_2O_3 to produce mullite at temperatures > 1200 °C. In the presence of Al, PDMS decomposition occurs in parallel with the oxidation of the metal and this results in redox side reactions that result in some elemental Si, before that in turn oxidises to SiO_2. Again reaction occurs between the oxidised PDMS and Al_2O_3 from the oxidised Al to form mullite. In earlier work,[7] we carried out a similar investigation of the phase evolution but with PMS as the starting polymer. Our results are broadly similar to those reported by Michalet et al. but with the following differences. First, Michalet reported the presence of transitional metastable Al_2O_3 crystal structures during the oxidation of Al and proposed that mullite formed by the reaction of these phases with SiO_2, however our data found that the transition phases transformed to α-Al_2O_3 prior to mullite formation. Second, Michalet reported extensive cristobalite crystallisation at intermediate temperatures, whereas our data found little cristobalite.

A major difference between the experiments carried out by Michalet et al.[6] and our previous work was in the size and morphology of the Al filler phase. Michalet et al. used a fine sub-micron sized spherical Al powder whereas in our earlier work a flake morphology Al was used of sub micron thickness but with a flake diameter of approximately 70 μm.[7] The current study has focused on the effect of the difference in Al powder characteristics (in terms of morphology and particle size) used as filler particles loaded in the PMS on the mullitisation temperature and mechanism of mullite formation.

2. Experimental, materials and method

Commercial PMS (0009465, Wacker Silicone Resin MK, Wacker-Chemie, Germany), a solid thermosetting siloxane polymer was used and loaded with 19 vol.% of Al powder as the active filler component. This PMS/Al ratio of 81/19 vol.% was determined using chemical formula, density data and chemical analysis data supplied by the manufacturers to determine the starting composition to form mullite of the desired stoichiometry, i.e. $3Al_2O_3{\cdot}2SiO_2$ or 3:2 mullite. A number of commercially available Al powders were selected to provide a range of powder size and morphology. Fig. 1 presents scanning electron microscope (SEM) micrographs of the

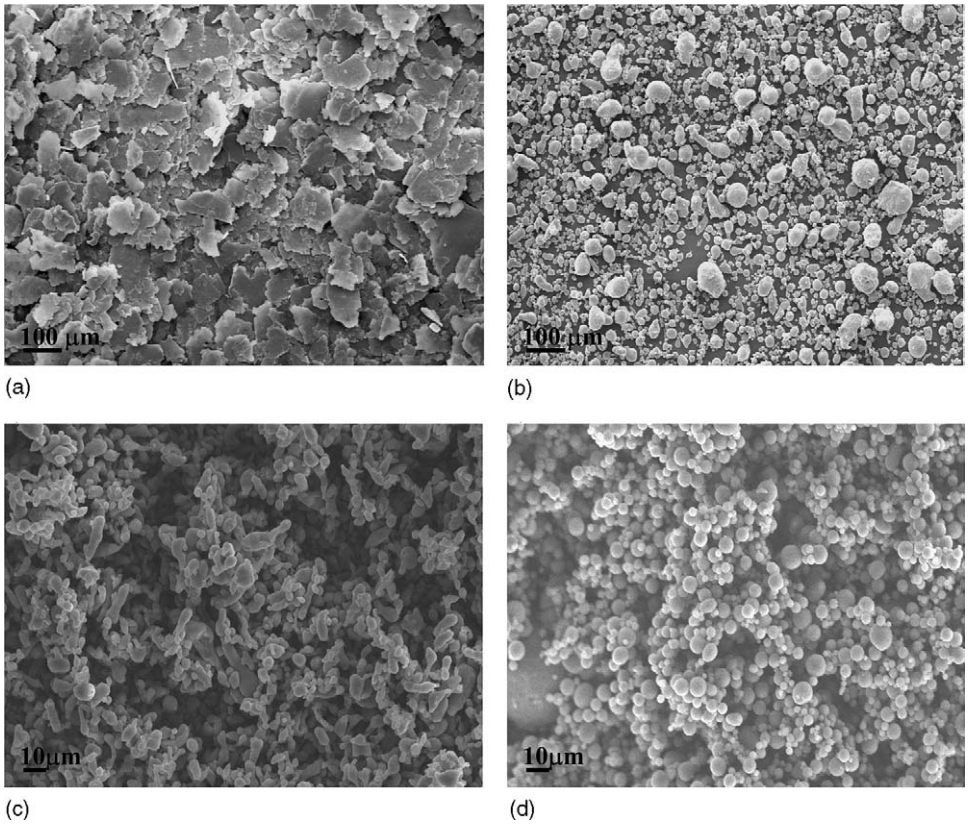

Fig. 1. Morphology of the Al powder samples (a) Merck flakes (B1), (b) Alfa Aesar (B2), (c) Alpoco irregular (B3) and (d) Alpoco spherical (B4).

Table 1
Particle size distribution of the Al used in the blend

Code no.	Supplier	Particle morphology	Mean particle size (μm)	Standard deviation (μm)	Distribution percentiles (μm)				
					10[a]	20[a]	50[a]	80[a]	90[a]
B1	Merck	Flakes	73 (<1)[b]	42	25	36	65	106	132
B2	Alfa Aesar	Spherical	56	48	17	24	45	78	103
B3	Alpoco	Irregular	9	4	4	5	8	12	14
B4	Alpoco	Spherical	10	7	4	5	8	13	17

[a] Volume.
[b] Thickness.

powders (Jeol 6300, Jeol, Tokyo, Japan) and Table 1 shows their particle size distributions as determined by laser light scattering (Mastersizer Microplus, Malvern Instruments, Great Malvern, UK). All the powders were at least 99 wt.% Al (manufacturers data, metal content) with the only significant impurity being approximately <1 wt.% Fe in the Merck and Alfa powders (B1 and B2). The Merck powder (B1) was the Al powder used in our earlier study of mullite formation.[7]

Samples were prepared by dissolving the PMS resin in ethanol:acetone, ratio of 95:5 vol.%, to which the Al powder was then added and stirred to obtain a homogeneous solution. Aluminium acetylacetonate ($Al(acac)_2$) (1 wt.%) was added as a catalyst (Sigma-Aldrich, Dorset, UK). After evaporating the solvent, coarse residual granulates were obtained and ground manually before sieving (100 mesh). The granulate (<150 μm) was then shaped in a die press at 200 °C and 15 MPa to cross-link the siloxane, yielding solid, dense cylindrical pellets of 16 mm diameter and ≈1.1 mm height. The pellets were converted into the corresponding ceramic samples by heat treatment in air, in a conventional chamber furnace. The heat treatment was as follows:

1. heating to 700 °C at 10 °C/min (0.167 °C/s),
2. isothermal hold for 2 h to oxidise the polymer,
3. heating to 1200 °C at 10 °C/min (0.167 °C/s),
4. isothermal hold for 10 h to convert the Al to the corresponding oxide,
5. heating to 1700 °C at 10 °C/min (0.167 °C/s),
6. 4 h isothermal hold.

Samples were removed from the furnace at different temperatures within the heat treatment and then cooled in air to room temperature for further analysis.

All samples removed at all stages from the above heat treatment were first subject to X-ray diffraction analysis (XRD) using Cu Kα radiation in a Philips PW3710 diffractometer (Philips, Eindhoven, Netherlands) to identify the crystalline phases present. Microstructures were investigated by SEM Jeol 6300 (Jeol, Tokyo, Japan) and Philips SEM525 (Philips, Eindhoven, Netherlands) equipped with an energy dispersive spectrometer (EDS; EDAX DX4). Further chemical analysis was carried out using a Cameca SX100 electron microprobe (Cameca, Paris, France).

Simultaneous thermal analysis (STA) consisting of thermal gravimetric analysis (TGA) and differential scanning calorimetry (DSC) (STA 449C, Netzsch, Selb, Germany) coupled to an evolved gas analysis (EGA) equipment, Thermostar™ model GSD 300T (Balzers, Litchenstein). All PMS/Al blends were studied to characterise the thermal decompositions and reaction process on heating the PMS/Al blends up to 1600 °C at a heating rate of 10 °C/min (0.167 °C/s) in an air atmosphere.

3. Results and discussion

3.1. Thermal analysis

Fig. 2a shows simultaneous TGA and DSC traces taken during the heat treatment in air from each of the four Al powders and also the PMS. There are a number of features common to all four Al powders. The endotherm on the DSC trace at 663–667 °C represents the melting temperature of Al. Oxidation is seen to occur in three distinct temperature regimes each of which has an exotherm on the DSC trace accompanied by a weight gain on the TGA. Point 3 characterises oxidation in the solid-state and is seen to be much more pronounced with the Al flakes sourced from Merck, indeed solid-state oxidation is almost negligible in the other three powder samples. The thin flake morphology of the Merck Al provides a greater specific surface area than in the other more equiaxed particle morphologies (Table 1 and Fig. 1). Oxidation of solid Al is slow and controlled by Al^{3+} ion diffusion through the protective aluminium oxide surface layer below the melting point.[8]

After melting, rupture of the oxide skin takes place and Al particles that are below a critical size completely oxidise, while those particles above the critical value merely develop an oxide shell.[9] Point 5 on the DSC trace represents this mechanism. All Al powder morphologies show significant weight gain, which scales with the specific surface area of the powders. The liquid-state oxidation of Al is seen to occur in two steps on the DSC traces in Fig. 2a. The further oxidation of the liquid Al (point 6) is a complex process controlled by the mechanical stability of the oxide film, the rupture of which controls the oxidation rate. Each Al powder shows different behaviour: complete oxidation of the flake morphology particles has occurred by 1400 °C with a weight gain of 85%, the irregular Alpoco particles showed complete oxidation by 1500 °C and a weight gain of 86%, the spherical Alpoco powder has not undergone complete oxidation by

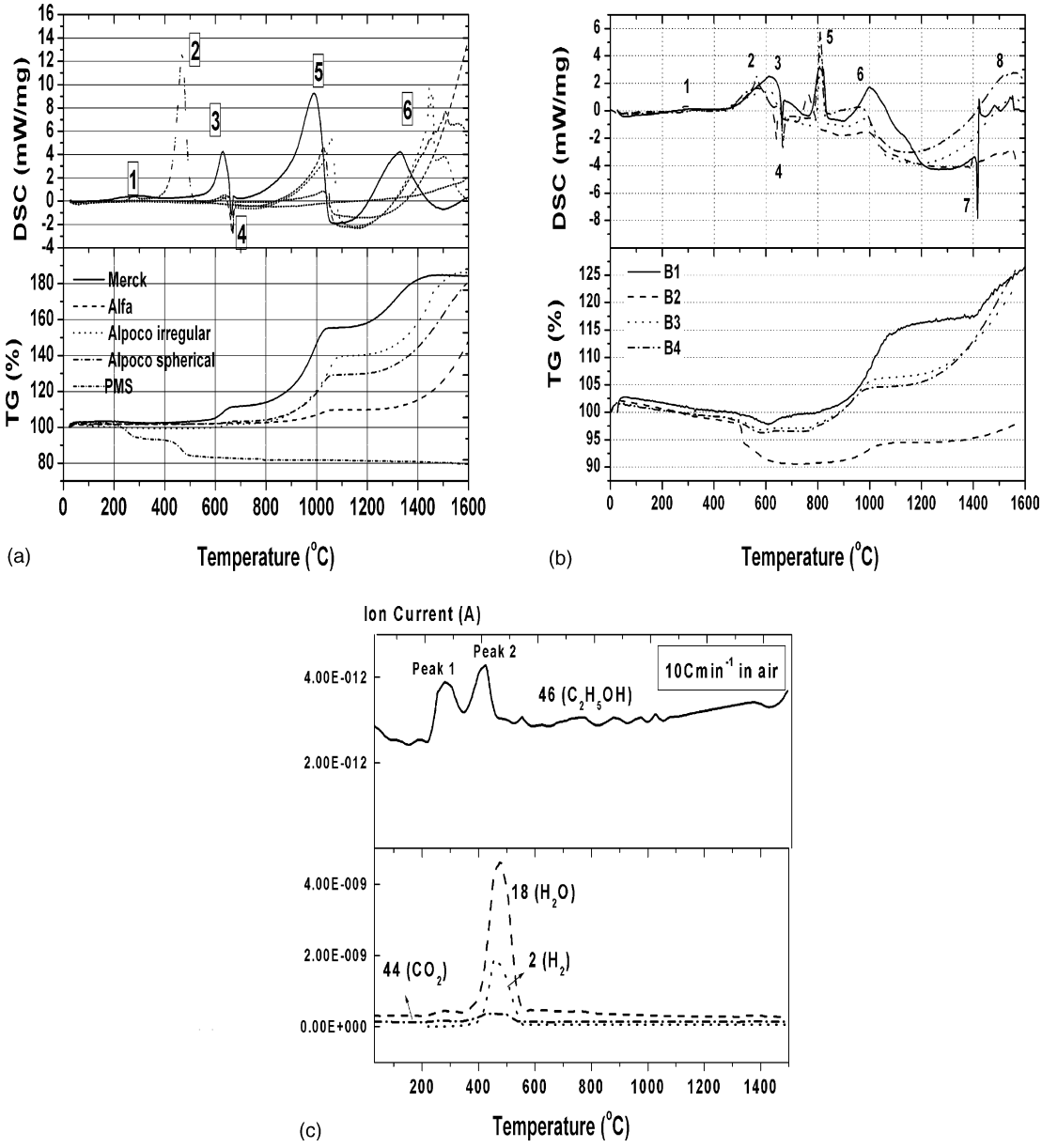

Fig. 2. Simultaneous thermal analysis (TGA and DSC) of (a) PMS and Al powders in isolation, (b) a range of PMS/Al powder mixtures and (c) EGA data obtained during the pyrolysis of PMS in air at a heating rate of 10 °C/min.

1600 °C and a weight gain of 80% was recorded, finally the Alfa Al powder recorded a weight gain of only 46% by 1600 °C. Again this behaviour correlates with the surface area of the powder samples.

Fig. 2a also shows the DSC and TGA traces from the PMS material in isolation. This has been discussed in detail in earlier work.[7] There is a weak exotherm (peak 1) and associated weight loss at 250 °C associated with a cross-linking reaction and a more intense exotherm (peak 2) and weight loss around 400–500 °C that characterises the pyrolysis of the cross-linked polymer, loss of organic side chains and conversion to an amorphous SiO_2 material.

Fig. 2b shows simultaneous DSC and TGA traces obtained from the PMS/Al mixtures (B1, B2, B3 and B4). These traces show a number of similarities with the DSC and TGA results of Fig. 2a. On the upper DSC trace, exothermic peak 1, believed to be associated with the cross-linking of the PMS, is shifted to a slightly higher temperature in all the PMS/Al mixtures. The exothermic peaks labelled 2 and 3 show significant variation between the PMS/Al samples and could be associated with a combination of the exothermic peak 2 in Fig. 2a seen at 469 °C with the PMS and peak 3 at 629 °C with the Al powder. Endothermic peak 4 is reasonably consistent and indicates the melting of the Al powder. At higher temperatures there are two further exotherms (peaks 5 and 6) accompanied by step weight gains on the TGA trace, these may be similar to the two exotherms associated with liquid Al oxidation (peaks 5 and 6 in Fig. 2a), but now they occur at significantly

lower temperatures. There are two further peaks evident on the DSC trace at higher temperatures. The sharply defined endotherm at 1416 °C (peak 7) occurs at the melting point of pure Si, the presence of Si was reported by Michalet et al.[6] and was also seen in our earlier work.[7] The exotherms that occur in the temperature range of 1450–1550 °C are thought to be associated with mullite formation. Most of the differences between the thermal analysis of the PMS/Al mixtures and of the PMS and Al in isolation can be explained by the increased availability of oxygen from the amorphous SiO_2. In particular, the small change in specimen weight seen around peak 5 (initial liquid stage oxidation of Al) indicates the possibility of a redox reaction with the amorphous product of PMS pyrolysis, which would result in elemental Si.

3.2. Phase evolution

Fig. 3 shows XRD traces taken from PMS/Al specimens after heat treatment to the indicated temperatures. Specimens B1 and B2 were examined over the full range of heat treatment from 400 to 1700 °C, B3 and B4 were investigated from 1200 to 1700 °C.

At 400 °C (Fig. 3a and b) the only crystalline phase present in samples B1 and B2 is Al. This is consistent with the slow

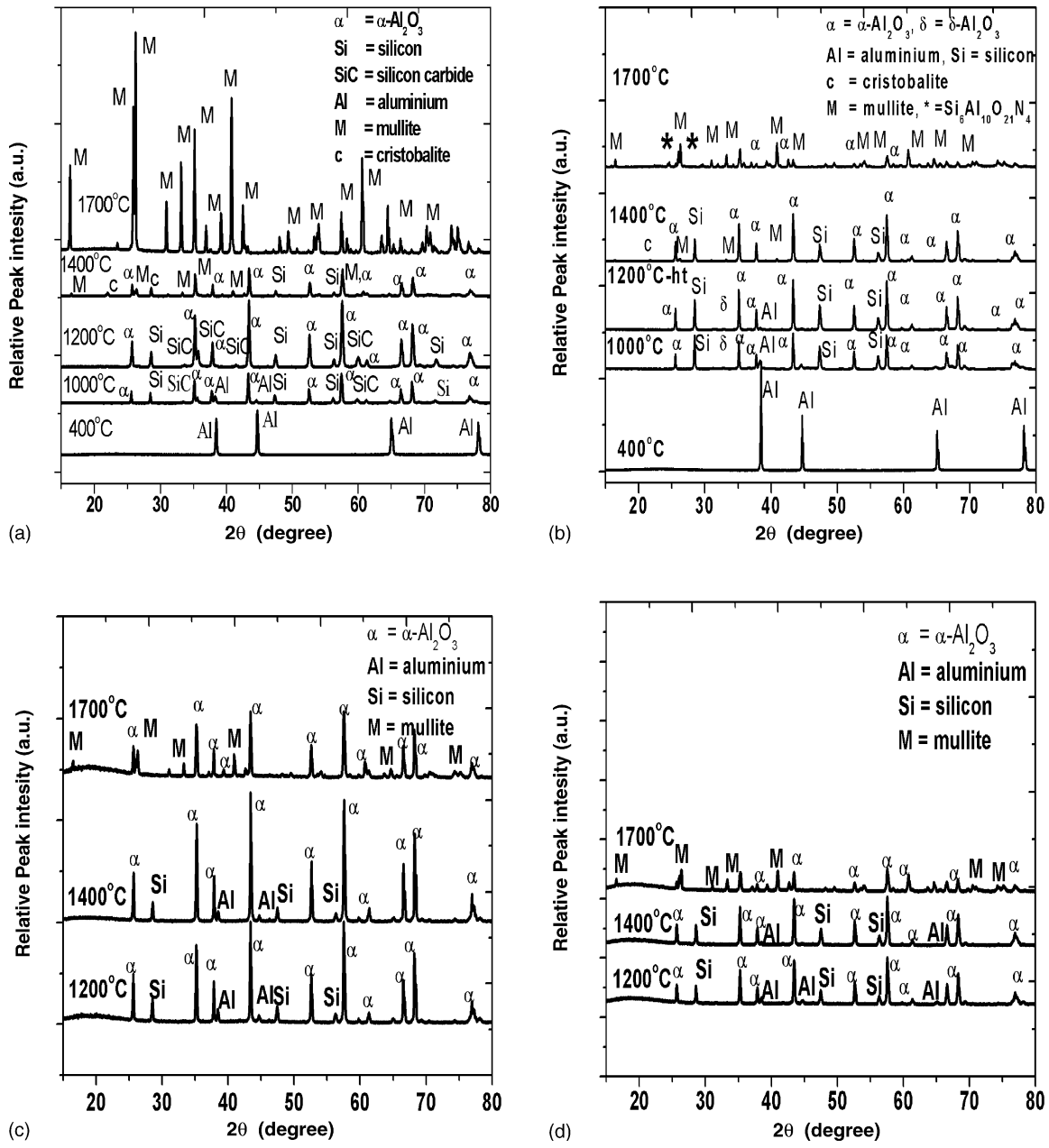

Fig. 3. XRD traces taken from PMS/Al samples after various heat treatment temperatures showing the presence of crystalline phases; (a) B1, Merck powder; (b) B2, Alfa powder (−ht = without 10 h holding time); (c) B3, Alpoco irregular powder; and (d) B4, Alpoco spherical powder.

rate of solid-state oxidation of Al at low temperatures and the amorphous products expected from degradation of the PMS. The XRD traces taken at 1000 °C show reduced Al content and now significant quantities of α-Al_2O_3 and Si. The presence of Si confirms the earlier interpretation of the STA results. Samples B1 and B2 are broadly similar at these two temperatures, however there are some additional very weak peaks identified as β-SiC in B1 and δ-Al_2O_3 in B2. As the intensities of both these signals are very weak, it is possible that both phases may exist in B1 and B2 but be below the detection limit for XRD. The presence of δ-Al_2O_3 is probably a relic of the early stage of solid-state oxidation of Al at low temperatures. In contrast with the report of Michalet et al.,[6] only small quantities of transition Al_2O_3 phases are found. SiC could form by reactions between the free Si, identified in both B1 and B2, with any carbon by-product of the decomposition of the PMS.

At 1200 °C all specimens showed α-Al_2O_3. Specimen B1 showed no residual Al and significant β-SiC, while specimens B2, B3 and B4 had significant retained crystalline Al. Crystalline Si was present in all samples as was reported by Michalet et al.[6] with pyrolysed PDMS/Al mixtures. They attributed the presence of Si to a redox process with the Al removing oxygen from the polymer. However, our TGA results suggest that the PMS has been substantially converted to an amorphous silica or silicon oxycarbide before significant oxidation of the Al has occurred. Suttor et al. also found from XRD and FTIR results that after an isothermal hold at 700 °C, amorphous SiO_2 is the only phase present besides Al_2O_3 in the PMS/Al_2O_3 mixture.[5] In addition to this, they reported the evaporation of gaseous SiO as a result of strong reducing effect of Al with respect to the Si–O bonds. Our TGA trace also detected this redox reaction with the formation of Si through a small weight gain at the first step of Al oxidation in the liquid-state (peak 5) shown in Fig. 2b. The presence of amorphous silica is confirmed later by the microstructural study using electron probe microanalysis. Thus, the reaction which proceeds to produce elemental Si is the reduction of the PMS pyrolysis products by metallic Al. We suggest three possible reaction pathways:

$$4\mathrm{Al} + 3\mathrm{SiO_2} \rightarrow 2\mathrm{Al_2O_3} + 3\mathrm{Si_{Al}} \quad (1)$$

$$4\mathrm{Al} + \frac{6}{x-y}\mathrm{SiO}_x\mathrm{C}_y \rightarrow 2\mathrm{Al_2O_3} + \frac{6y}{x-y}\mathrm{CO}\uparrow + \frac{6x}{x-y}\mathrm{Si_{Al}} \quad (2)$$

$$4x\mathrm{Al} + 6\mathrm{SiO}_x\mathrm{C}_y \rightarrow 2x\mathrm{Al_2O_3} + 6y\mathrm{SiC} + 6(1-y)\mathrm{Si_{Al}} \quad (3)$$

where the subscript Al represents Si in solution in liquid Al. Because of the uncertain composition of the SiO_xC_y these reactions are necessarily schematic and will depend strongly on the local oxygen partial pressure. However, the free energy of formation of Al_2O_3 at a standard pressure at 1000 °C is significantly lower than that of SiO_2 as found in the Ellingham diagram[11] and thus the reduction of silica or the oxycarbide composition is likely. By 1400 °C significant differences can be seen in the phase evolution of the four samples. In specimen B1, the Si peak is much less intense than was the case at 1200 °C, some of the SiO_2 has transformed to cristobalite and significant quantities of mullite are recorded. In parallel with the formation of mullite, the α-Al_2O_3 signal is also reduced. In specimen B2, the α-Al_2O_3 and Si peak intensities are similar to those at 1200 °C, there is a weak cristobalite and there is a weak mullite signal measurable. In contrast, specimens B3 and B4 show α-Al_2O_3, retained Al, Si peaks and no detectable mullite. After final heat treatment to 1700 °C, all specimens showed the formation of mullite. Sample B1 showed no other crystalline phases present while specimens B2, B3 and B4 all showed significant Al_2O_3. In specimen B2, a small quantity of a third phase, tentatively identified as a Sialon ($Si_6Al_{10}O_{21}N_4$), was found.

3.3. Microstructures and phase distribution

Fig. 4 shows microstructures from specimens B1, B2 and B3 after heat treatment to 400 °C. At this temperature the PMS matrix is fully cross-linked but thermal decomposition has yet to begin. Sample B4 showed a microstructure essentially identical to that of B3. The composite nature of the mixture is evident with the microstructure controlled by the morphology of the Al powder. The basic microstructural features determined after cross-linking the PMS are retained to higher temperatures as can be seen in Fig. 5, which shows the microstructure after heat treatment to 1000 °C. There is now a significant volume fraction of voids present, these are believed to have formed during the pyrolysis of the PMS when substantial mass loss and transformation to an inorganic amorphous matrix leads to shrinkage and its accommodation by the development of internal voids. These voids are believed to be a continuous interlinked network providing a path for easy oxygen access throughout the material. In Fig. 5b, finer details of the microstructure are revealed. From the XRD results in Fig. 3a, the crystalline phases expected are α-Al_2O_3, Al and Si. From microanalysis results (Fig. 6) the discontinuous grey phase is tentatively identified as α-Al_2O_3 in an amorphous matrix, the bright white phase may be elemental Si.

Fig. 6 shows elemental maps produced from regions near the surface of sample B1 using electron probe microanalysis after heat treatment to 1000 °C. Fig. 7 shows regions of the same specimen taken from the sample centre. In both figures regions of high Al content, with no Si or O present, indicate unoxidised Al. There are similar regions with high Si content and no Al or O, these confirm the presence of elemental Si inferred earlier from the DSC and XRD data.

Oxidation to Al_2O_3 occurs preferentially on the laminar defects (resulting from the initial compact of the Al flakes) allowing easy access to the furnace atmosphere (Figs. 5b and 6c).

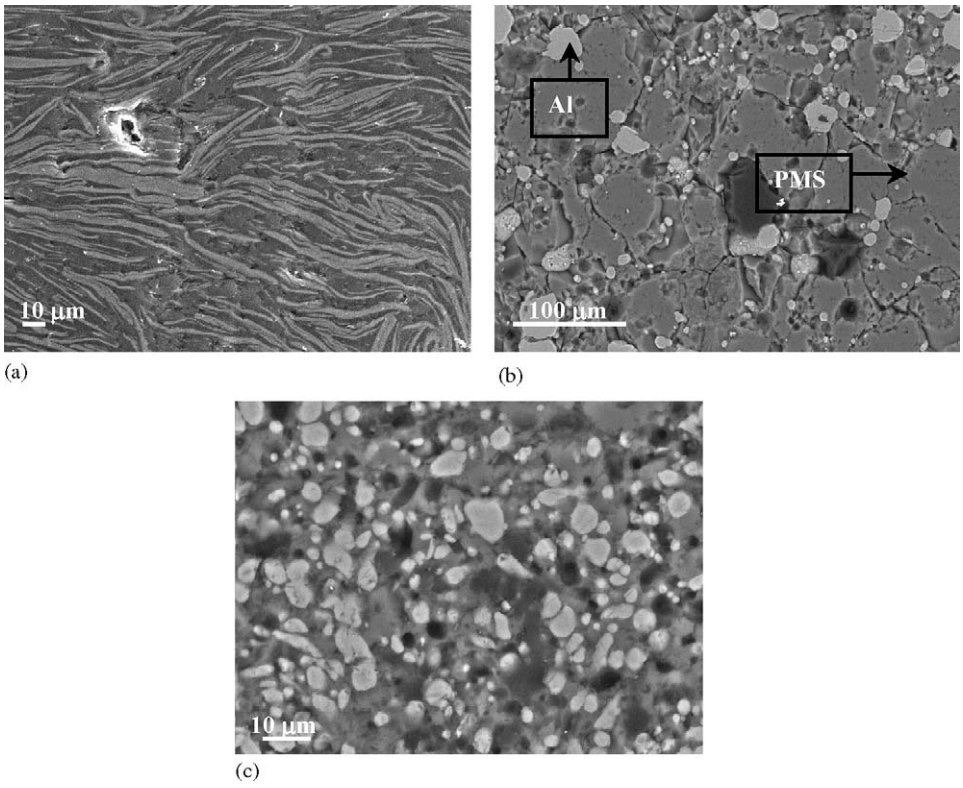

Fig. 4. SEM micrographs in back scattered electron mode of a cross section of sample (a) B1, (b) B2 and (c) B3 after heating to 400 °C (bright phase = Al and dark phase = PMS).

The relationship between the components of the pyrolysed sample at 1000 °C is more clearly distinguishable in the series of higher magnification images from the specimen interior given in Fig. 7. Five regions are delineated on the images of cross section of sample B1. In general, Al concentration appears to be stratified at three concentrations shown as green, yellow and red. The black or blue region correlates with porosities in the BSE image and is taken as indicating zero Al concentration. Si is predominantly at orange/red and blue with small regions at green or yellow. The oxygen map (Fig. 7d) shows the greatest variation in concentration and over the shortest length scales. The regions of highest Al concentration (e.g. region 4) correlate with low O and Si content and are believed to be remnants of the Al flakes, which have melted and re-solidified. The regions of highest O content (e.g. just above region 3) correlate with intermediate Al contents and are believed to indicate the presence of Al_2O_3. These regions were always close to the edges of porosities (SEM BSE image in Fig. 7a) as can be seen with the other high O region in area 5. Area 3 (high Si, very low Al and O) probably indicates a region of elemental Si. Areas 1 and 2 contain a mixture of Al, Si and O with area 2 richer in Si compared to area 1 (lower in oxygen content), this is taken to represent the amorphous matrix region of mixed oxides.

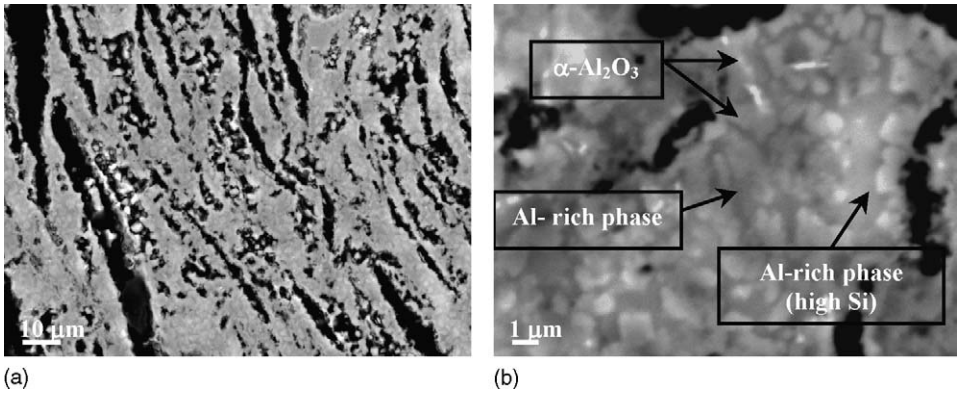

Fig. 5. BSE images of specimen B1 after heating to 1000 °C: (a) cross-section and (b) higher magnification image showing constituent phases.

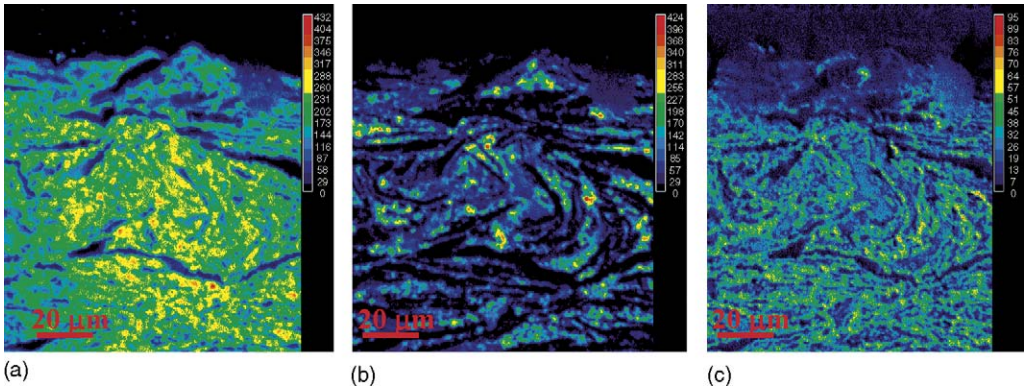

Fig. 6. Elemental maps with WDS of sample B1 after heating to 1000 °C at surface: (a) Al map, (b) Si map and (c) O map.

Regions of blue colour in Si map correlate with regions of blue colour in O map indicating the areas of amorphous SiO_2. On reaching 1400 °C, the EPMA results (Fig. 8) show the regions of high Al content correlate with high O indicating that the Al is indeed fully oxidised. There are still some small regions of elemental Si indicated by the red spots on Fig. 8b.

Fig. 9 shows EPMA results from specimen B2 after heat treatment to 1000 °C. It shows a highly cracked microstructure. This may indicate that the structure of coarse packed Al spheres in a cross-linked PMS matrix is less able to accommodate shrinkage stresses than the laminar microstructure seen in specimen B1. Re-examining the microstructures after

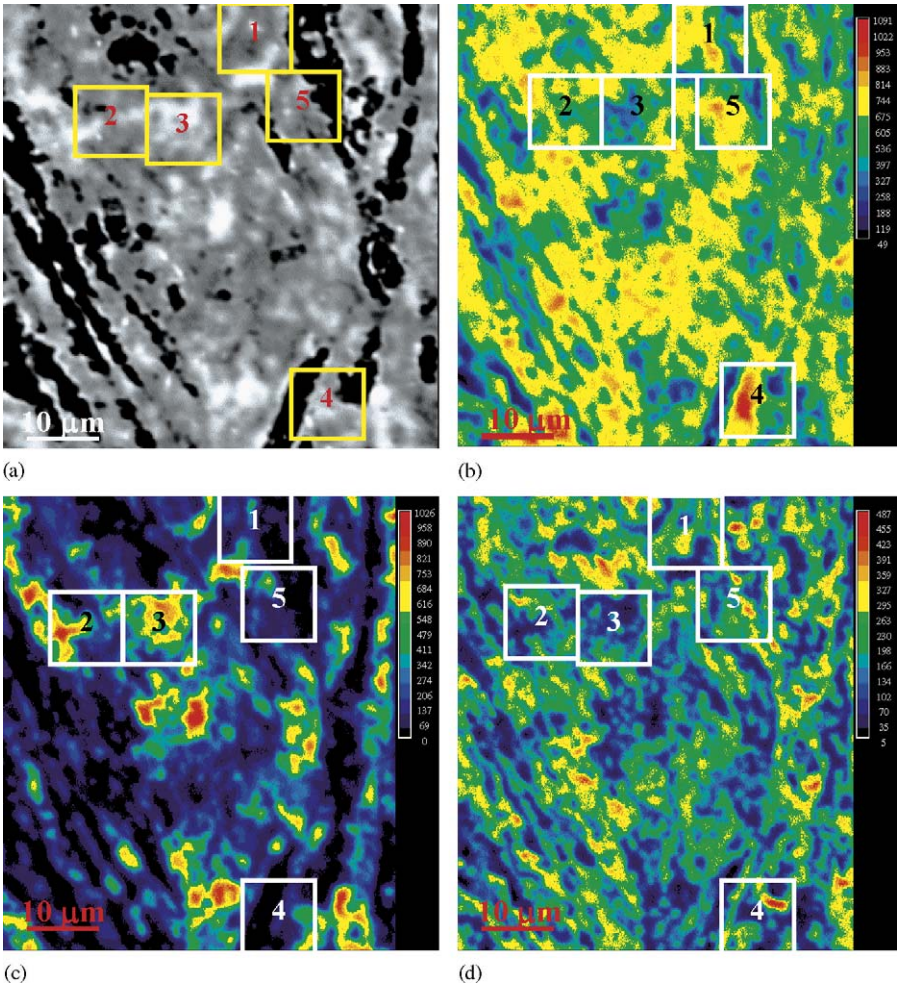

Fig. 7. Elemental maps with WDS of sample B1 after heating to 1000 °C: (a) BSE image, (b) Al map, (c) Si map and (d) O map.

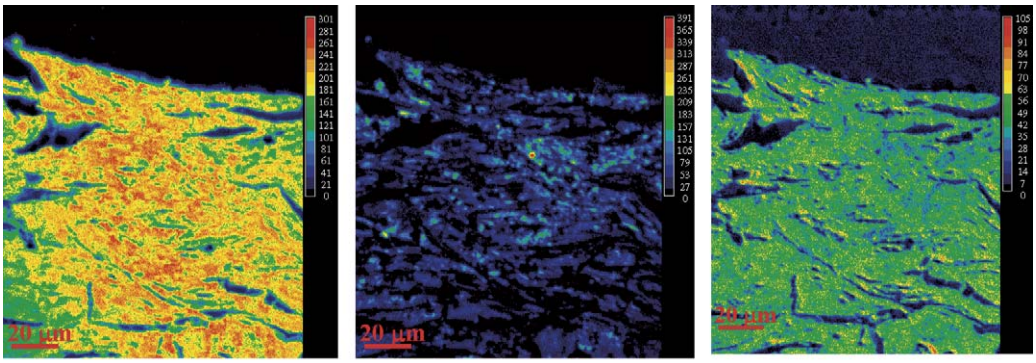

Fig. 8. Elemental maps with WDS of B1 1400 °C sample at surface: (a) Al map, (b) Si map and (c) O map.

heat treatment to 400 °C (Fig. 4) indicates cracking already present in specimen B2 while specimens B1 and B3 are crack free. The three elemental maps in Fig. 9a–c show an inhomogeneous composition after heat treatment. In Fig. 9b, islands of elemental Si are clearly visible near the specimen surface and absent in the interior. Surrounding the Si islands is a region of higher Al content. The interior of the specimen shows lower Al content and here the regions of high Si content correlate with high O content and the absence of Al, indicating that these regions have a composition SiO_2. We hypothesise that the highly cracked microstructure allowed Al flow above its melting point and that in these regions of higher Al content there will be reduced access of O from the furnace atmosphere and the Al metal reduces the local SiO_2 content to elemental Si. Regions where SiO_2 is retained do not contain significant unoxidised Al. Elemental maps from the specimen heated to 1400 °C are given in Fig. 10. Significant regions of elemental Si (red/orange colouration) are visible consistent with the XRD data. Comparing the Al and Si elemental maps in both locations show that the intermediate Si levels (blue) correlate with regions of high Al and O content. This indicates that temperature increase to 1400 °C leads to the complete oxidation of the Al-rich matrix, which leads to Si (which is dissolved in Al melt) being rejected on the boundaries. Comparing Fig. 10b and e shows a region of Si depletion near the surface which might be the result of volatilisation of SiO from the reaction of Si and SiO_2[12] as seen by Suttor et al. in the temperature range of 700–1200 °C.[5]

The microstructures and phase distribution seen in both Alpoco sourced powders were essentially identical, the results for B3 are presented here. EPMA results from the specimen surface of specimen B3 heat-treated to 1400 °C are given in Fig. 11a–c and d–f for the interior. There are a number of similarities with specimen B2 in that the surface region of the specimen is clearly depleted in Si, although some regions of elemental Si are visible in Fig. 11b. The Al map from the central region (Fig. 11d) shows regions of high Al concentration that correlate with zero Si and O, indicating the presence of small regions of elemental Al. This is consistent with the XRD data showing retained Al in specimens B3 and B4 at these temperatures (Fig. 3c and d).

Finally, in Fig. 12, we can see the presence of elongated mullite crystals in an amorphous matrix in specimens B1, B2 and B3 after heat treatment to1700 °C. In Fig. 12a, the microstructure from sample B1 shows an extensive interlocking network of 3:2 mullite grains in an amorphous matrix. EDS measurements on the surrounding matrix

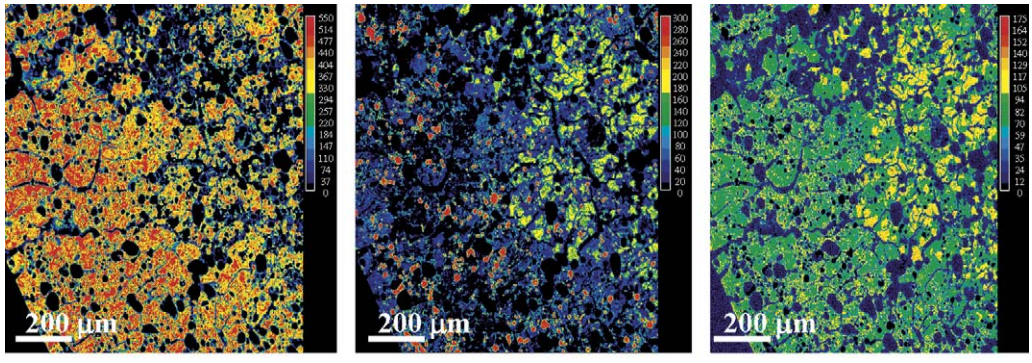

Fig. 9. Elemental maps with WDS of sample B2 after heating to 1000 °C: (a) Al map, (b) Si map and (c) O map.

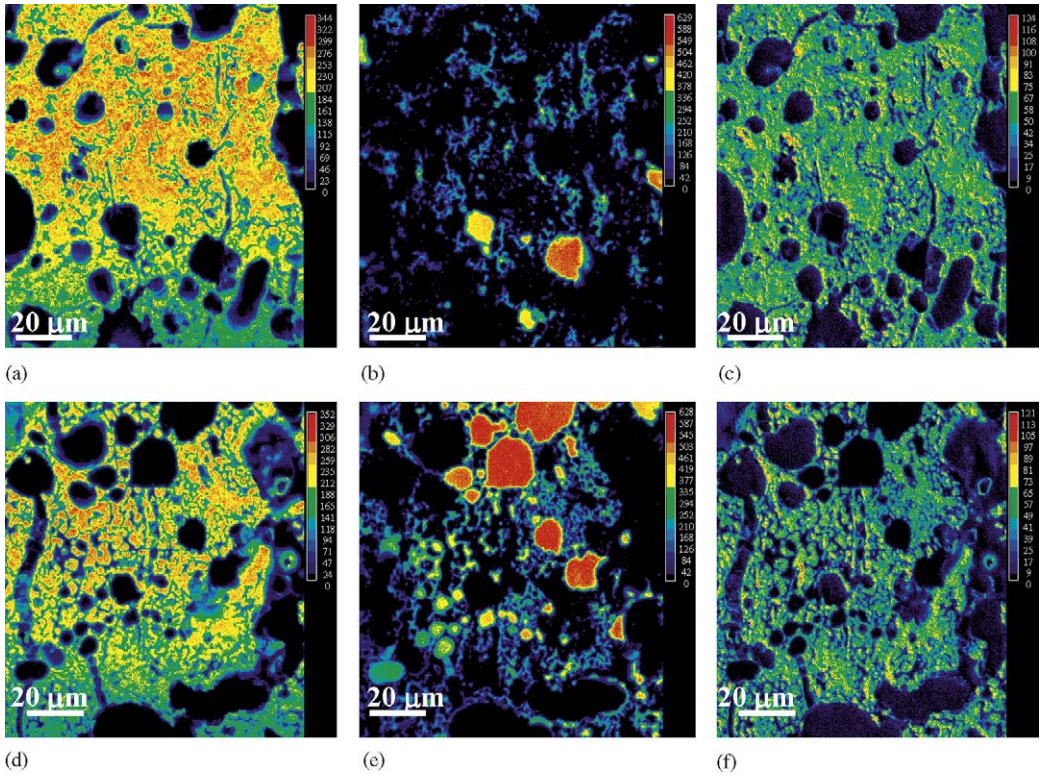

Fig. 10. Elemental maps with WDS of sample B2 after heating to 1400 °C: (a–c) from the surface region and (d–f) from the interior region: (a and d) Al map, (b and e) Si map and (c and f) O map.

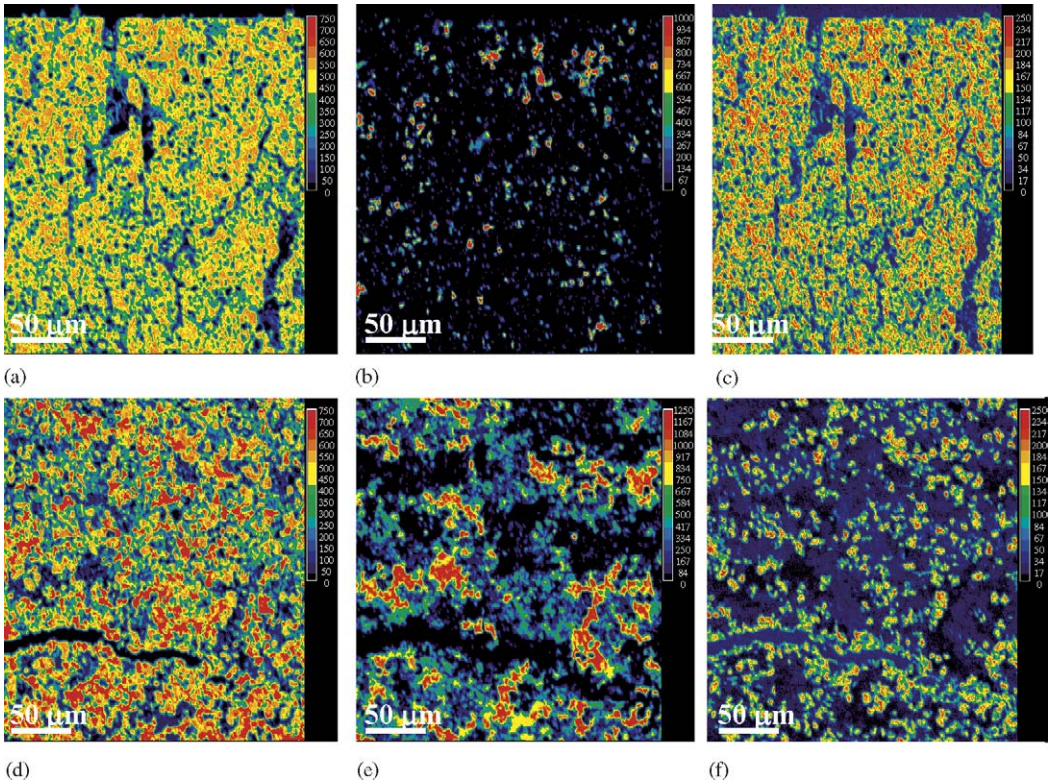

Fig. 11. Elemental maps with WDS of sample B3 after heating to 1400 °C: (a–c) from the surface region and (d–f) from the interior region: (a and d) Al map, (b and e) Si map and (c and f) O map.

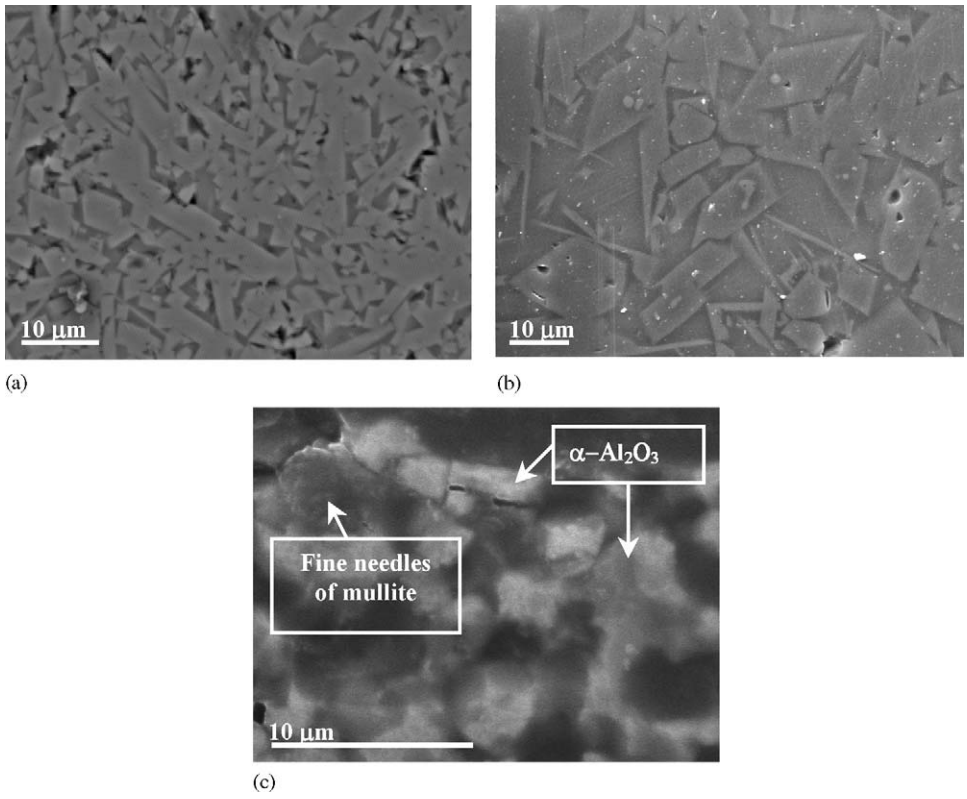

Fig. 12. SEM images of samples heat treated to 1700 °C showing mullite grains in an amorphous matrix, (a) B1 in BSE mode, (b) B2 in SE mode and (c) B3 in BSE mode.

found it to be of variable composition with either a Si or Al excess. A similar microstructure was found with specimen B2, although there was less mullite present and the mullite grains are larger than in B1. Individual grains of Al_2O_3 or other phases identified by XRD could not be resolved. Specimen B3 shows a more complex microstructure (Fig. 12c) with a few needle-like grains (very faint grains in the dark phase) distributed among more equiaxed α-Al_2O_3 grains (bright phase). The needle-like grains are presumed to be mullite but they were too small to allow spot EDS analysis.

4. Discussion

There are several possible pathways or steps in the mechanisms leading to mullite formation from PMS/Al mixtures. There is a clear influence of starting Al powder on these, as can be seen in Fig. 3 by the different temperatures at which intermediate phases form and by the presence or absence of presumed side-reaction products such as SiC and Sialon. There are two ways in which the size and shape of the starting Al powder can influence the subsequent sequence of reactions leading to mullite formation. First, as is clearly shown in Fig. 2a, each of the four powders has a different rate of oxidation in both the solid and liquid states. Second, the presence of solid Al particles in the Al/PMS composite strongly influences the microstructure, in terms of the internal void network, after initial pyrolysis of the PMS at temperatures below those that lead to significant oxidation of the Al. The nature of this internal void structure will be critical in ensuring adequate oxygen transport to allow the formation of SiO_2 and Al_2O_3 throughout the specimen before mullitisation can occur.

We propose that the fine Alpoco powders (B3 and B4) produce a very different composite structure than was found with either the Merck (B1) or Alfa (B2) powders despite these larger particles having a very different morphology to each other. From the EPMA data taken at 1400 °C (Fig. 11a), and from the XRD evidence of retained Al (Fig. 3c and d) it would appear that these specimens have had restricted access of O_2 into the specimen interior. Neither B1 nor B2 showed evidence for poor oxygen access. In the case of specimen B1 this may be because the flake morphology of the starting Al resulted in a particularly favourable structure for O_2 access. The resulting microstructure of laminar cracks is clearly retained to 1000 °C (Fig. 5) and may even be visible at 1400 °C (Fig. 8). In the case of specimen B2, it may be the large size of the Al particles that leads to the extensive network of cracks seen in the microstructure (Fig. 9). These cracks would act as a pathway for O_2 ingress but they may also allow migration of liquid Al, which could explain the segregation seen in Fig. 9. Another difference between the specimens that may be accounted for by the void structure is

the loss of Si from the surface regions at temperatures around 1400 °C.

Samples B1 and B2 show the onset of mullite formation at temperatures between 1200 and 1400 °C, whereas in samples B3 and B4 no mullite is observed until temperatures above 1400 °C. One of possible reasons for this could be because the structure in specimens B3 and B4 does not provide access for enough O_2 to transform the elemental Si to SiO_2 to react with Al_2O_3. Comparing Si distribution maps from samples heat treated to 1400 °C (Figs. 8b, 10b and 11b) it is clear that specimen B1 has the largest quantity of SiO_2 (Fig. 8b). They also show that the greatest degree of Si depletion has occurred in specimen B3 (Fig. 11b) and that ease of mullite formation scales with extent of Si retention after heat treatment. It is also possible that the earlier oxidation of the Al flakes in sample B1, and the retention of flake morphology after melting, may lead to a better distribution of Al_2O_3 for mullite formation. Note that Michalet et al.,[6] using sub-micron Al powder, also found mullite formation at very low temperatures and there starting material would also result in a fine dispersion of Al_2O_3. However, in contrast to Michalet, no transition aluminas were found in this study. The likely reaction mechanism for mullite formation at low temperature (<1400 °C) in sample B1 and possibly B2 is the reaction between α-Al_2O_3 and amorphous SiO_2. When cristobalite crystals are available from crystallisation of amorphous SiO_2[10,13] (seen in Fig. 3a and b), mullite can also be formed via a solid-state reaction between cristobalite and Al_2O_3. This is the second mechanism of mullite formation in sample B1. Further increase in temperature above 1650 °C causes melting of cristobalite or to form SiO_2-rich liquid (above eutectic in the Al_2O_3–SiO_2 system) and liquid-phase-assisted sintering mechanism becomes dominant in promoting mullitisation at this temperature.[5,10] In samples B3 and B4, mullite formation is delayed to higher temperatures.

Finally, the influence of the side redox reaction that results in elemental Si must not be ignored. Mullite is believed to form by an interdiffusion reaction between α-Al_2O_3 and SiO_2 containing material (either amorphous matrix or cristobalite crystals). However, because of differences in reaction kinetics, the PMS converts to SiO_2 at a temperature below that at which significant oxidation of the metallic Al occurs. Thus, there is the opportunity for a redox reaction, which oxidises the Al but reduces the SiO_2 to elemental Si. This reaction path occurs in all four Al samples investigated here and was reported by Michalet et al.[6] who used PDMS as the Si source. As can be seen from the EPMA results, the size of the Si inclusions that result from this redox process scale with the microstructure, which is in turn controlled by the Al particle size. Hence the size of the Si inclusions scales from specimen B2 containing the largest to B1 the smallest. In all these cases, the size of the Si inclusions (typically > 10 μm) will significantly delay the final oxidation of the components to temperatures > 1400 °C (the melting temperature of Si).

5. Conclusions

Active filler pyrolysis of PMS/Al mixtures results in the formation of mullite ceramics with initial mullite formation possible at temperatures < 1400 °C, however, complete mullitisation does not occur until temperatures close to 1700 °C. The reaction route is complex with intermediate stages of Si, SiO_2 and Al_2O_3. Side reactions may result in the formation of other unwanted phases, e.g. SiC. The size and morphology of the starting Al powder controls the reaction pathway and kinetics, with the ease of Al particle oxidation being inversely proportional to its size. From our results, which found that the starting Al powders with the largest dimensions (B2: Alfa spherical particles with diameter >50 μm) and the smallest dimensions (B1: Merck flakes with flake thickness <1 μm) gave the most complete mullitisation, we can conclude that it is the structure of the Al/PMS compact that has the most influence on reaction efficiency. This is because in samples B1 and B2 there was an interconnected network of voids from the specimen surface to the interior retained at temperatures in excess of 1400 °C. The result for specimen B2 was particularly striking as when this Al powder was oxidised in isolation, incomplete oxidation occurred in the TGA experiments at temperatures up to 1600 °C. In samples B3 and B4, the smaller spherical Al particles seemed to block the access of O_2 to the specimen interior.

Acknowledgements

J.A. would like to acknowledge the financial support of Alstom Power and the University of Manchester for an OSS award.

References

1. Greil, P., Seibold, M. and Erny, T., *Microcrystalline Ceramic Composites by Active Filler Controlled Reaction Pyrolysis of Polymers in Materials Research Symposium, Vol 274*, ed. H. Schmidt and K. Hirano. MRS, Pittsburgh, 1992, pp. 155–166.
2. Erny, T., Seibold, M., Jarchow, O. and Greil, P., Microstructure development of oxycarbide composites during active-filler-controlled polymer pyrolysis. *J. Am. Ceram. Soc.*, 1993, **76**(1), 207–213.
3. Greil, P., Active-filler-controlled pyrolysis of preceramic polymers. *J. Am. Ceram. Soc.*, 1995, **78**(4), 835–848.
4. Greil, P., Near net shape manufacturing of polymer derived ceramics. *J. Eur. Ceram. Soc.*, 1998, **18**, 1905–1914.
5. Suttor, D., Kleebe, H. J. and Ziegler, G., Formation of mullite from filled siloxanes. *J. Am. Ceram. Soc.*, 1997, **80**(10), 2541–2548.
6. Michalet, T., Parlier, M., Beclin, F., Duclos, R. and Crampon, J., Elaboration of low shrinkage mullite by active filler controlled pyrolysis of siloxane. *J. Eur. Ceram. Soc.*, 2002, **22**, 143–152.
7. Anggono, J. and Derby, B., Intermediate phases in mullite synthesis via aluminium and alumina filled polymethylsiloxane, *J. Am. Ceram. Soc.*, submitted for publication.
8. Wefers, K. and Misra, C., *Oxides and Hydroxides of Aluminium*. Pittsburgh Alcoa Laboratories, Pittsburgh, 1987.

9. Gaus, S. P., Chan, H. M., Harmer, M. P. and Caram, H. S., *Temperature Runaway and Scale-up of the Reaction Bonding of Aluminium Oxide*, *Vol 79*, ed. K. V. Logan, Z. A. Munir and R. M. Spriggs. American Ceramic Society, 1996, pp. 237–246.
10. Saruhan, B., Albers, W. and Kaysser, W. A., Reaction and sintering mechanisms of mullite in the systems cristobalite/α-Al_2O_3 and amorphous SiO_2/α-Al_2O_3. *J. Eur. Ceram. Soc.*, 1996, **16**, 1075–1081.
11. Gaskell, D. R., *Introduction to the Thermodynamics of Materials* (*3rd ed.*). Taylor & Francis, Washington, DC, 1995, p. 370.
12. Pearce, C. A., *Silicon Chemistry and Applications*. The Chemical Society, London, 1972.
13. Nurishi, Y. and Pask, J. A., Sintering of α-Al_2O_3/amorphous silica compacts. *Ceram. Int.*, 1982, **8**, 57–59.